CEBAF PROPOSAL COVER SHEET

This Proposal must be mailed to:

CEBAF
Scientific Director's Office
12000 Jefferson Avenue
Newport News, VA 23606

and received on or before 1 October 1991.

A. TITLE:

Measurement of Polarized Structure Functions in Inelastic Electron Proton Scattering using the CEBAF Large Acceptance Spectrometer

B. CONTACT PERSON:

Volker Burkert

ADDRESS, PHONE, AND ELECTRONIC MAIL ADDRESS:

CEBAF
Newport News, VA
BURKERT @ CEBAFVAX
804-249-7540

C. IS THIS PROPOSAL BASED ON A PREVIOUSLY SUBMITTED PROPOSAL OR LETTER OF INTENT?

[ ] YES [x] NO

IF YES, TITLE OF PREVIOUSLY SUBMITTED PROPOSAL OR LETTER OF INTENT:

****

(CEBAF USE ONLY)

Receipt Date 1 OCT 91

Log Number Assigned PR 91-023

By [redacted]

Measurement of Polarized Structure Functions in Inelastic Electron Proton Scattering using the CEBAF Large Acceptance Spectrometer

Spokespersons: V. Burkert, D. Crabb, R. Minehart

The N^* Group in the CLAS Collaboration

V. Burkert, D. Joyce, B. Mecking, M. Mestayer, B. Niczyporuk, E. Smith, A. Yegneswaran
CEBAF, Newport News, Virginia

D. Crabb, D. Day, R. Marshall, J. McCarthy, R. Minehart
O. Rondon-Aramayo, R. Sealock, L.C. Smith, S. Thornton, H.J. Weber
University of Virginia, Charlottesville, Virginia

P. Stoler, G. Adams, N. Mukhopadyay
Rensselaer Polytechnic Institute, Troy, New York

K. Beard, C. Carlson, H. Funsten
College of William and Mary, Williamsburg, Virginia

D. Isenhower, M. Sadler
Abilene Christian University, Abilene, Texas

D. Doughty, D. Heddle
Christopher Newport College, Newport News, Virginia

L. Dennis, A. Tam
Florida State University, Tallahassee, Florida

S. Dytman, T. Donoghue
University of Pittsburg, Pittsburg, Pennsylvania

J. Lieb
George Mason University, Fairfax, Virginia

K. Giovanetti
James Madison University, Harrisonburg, Virginia

M. Manley
Kent State University, Kent, Ohio

C. Stronach
Virginia State University, Petersburg, Virginia

M. Gai
Yale University, New Haven, Connecticut

Abstract

An experiment to study polarized structure functions in inelastic electron scattering using a polarized solid state $^{15}NH_3$ target and the CEBAF Large Acceptance Spectrometer is proposed. The experiment measures the inclusive polarized structure functions, A_1 and A_2, in a range of $0.2 < Q^2 < 1.5\ GeV^2$, and $1.1 < W < 1.8\ GeV$. The impact of the measurement on the determination of the Q^2 evolution of the Gerasimov-Drell-Hearn Sum Rule, and on the determination of the photo-coupling amplitudes of the Roper resonance are discussed in detail. A detailed comparison of the results assuming that the Roper resonance $P_{11}(1440)$ is a regular radially excited 3-quark (q^3) state as suggested by the non-relativistic quark model, or, alternatively the ground state of a hybrid system ($q^3 - G$) with a valence gluon, as suggested by some recent model calculations, is given. The measurement will be the first significant double polarization measurement in the nucleon resonance region.

I. Introduction

The study of the hadronic structure of baryons at CEBAF will be significantly enhanced through the use of a polarized electron beam and polarized targets. In inclusive electron scattering, it is possible to measure two new structure functions, A_1 and A_2, which are not accessible without the use of the spin degrees of freedom [CLO78]. In inelastic scattering, the structure function A_1 is of particular interest. A_1 is directly related to $\sigma^T_{1/2} - \sigma^T_{3/2}$, the difference in the total transverse absorption cross sections for helicity 1/2 and helicity 3/2 in the γ_v - nucleon system. The measurement of this structure function in the deep inelastic region by the CERN EMC [ASH88] collaboration led to numerous speculations about the nucleon spin possibly being carried not by the quarks but by the glue. A measurement A_1 in the region of the nucleon resonances yields information about the spin properties of the electromagnetic transition form factor for baryon resonances. The measurement can also be used to establish the Q^2 evolution of the Gerasimov-Drell-Hearn sum rule [GER65],[DRE66] and its relationship to the deep inelastic regime (duality).

CLAS is well matched for polarized target experiments; especially since only moderate luminosity can be achieved both for polarized solid state targets [MEY85, WPT84], and for polarized gas targets. Solid state polarized hydrogen (and deuterium) targets are limited in the amount of electron beam intensity that they can withstand without significant radiation damage. The maximum luminosity is limited to about $\simeq 5 \times 10^{34}$ cm^{-2}sec^{-1} for radiation resistant ammonia targets (the luminosity is given in terms of the total number of nucleons in the target including the nitrogen host material). This limit is actually well matched to the expected luminosity limitation of the CLAS. The large acceptance of the CLAS detector is important in achieving reasonable count rates with these targets, even in inclusive experiments.

The design of the CLAS detector is well suited for use with a solid state polarized target. The nearly zero field on axis provided by the CLAS magnet does not disturb the operation of the target. The 5 Tesla holding field associated with hydrogen and deuterium solid state polarized targets does deflect both the electron beam and the reaction products (such as the scattered electron) significantly, but the particle trajectories can be reconstructed to retrieve the kinematic quantities of interest.

In Section II, we outline the methods that we propose to determine the inclusive polarized structure functions A_1 and A_2. Some specific problems of using polarized solid state targets with CLAS are discussed in Section III.

II. Polarized Structure Functions in Inclusive Electron Scattering

The differential cross section for inclusive scattering of polarized electrons off polarized protons $\vec{p}(\vec{e},e')X$ can be expressed in the following way:

$$\frac{d\sigma}{d\Omega_e dE'_e} = \Gamma_T \cdot$$

$$[\sigma_T + \epsilon\sigma_L + P_e \cdot P_p \cdot cos\phi \cdot (\sqrt{1-\epsilon^2} \cdot cos\psi \cdot A_1 \cdot \sigma_T + \sqrt{2\epsilon(1-\epsilon)} \cdot sin\psi \cdot A_2 \cdot \sigma_T)] \quad (1)$$

where $\vec{P}_e$ and $\vec{P}_p$ are the electron and target polarizations, respectively, ψ is the angle between $\vec{P}_p$ and the direction of the virtual photon, and ϕ is the azimuthal angle between the electron scattering plane and the target polarization vector(Figure 1). The two polarization structure functions, A_1 and A_2, can be separated by polarizing the target in the scattering plane ($\phi = 0$), and by varying the polarization angle ψ for fixed electron kinematics. However, since we are mostly interested in the structure function A_1 we propose in the following section a method to measure A_1 which does not require changing the orientation of the target polarization with respect to the beam axis.

II.1 Separation of the Polarization Structure Functions A_1 and A_2

In the proposed experiment the target nucleon is polarized along the electron beam axis. Therefore, ψ in (1) becomes the angle θ_γ of the virtual photon relative the beam axis, and $\phi = 0.^\circ$ Consequently the relation (1) is transformed into:

$$\frac{d\sigma}{d\Omega_e dE'_e} = \Gamma_T \cdot$$

$$[\sigma_T + \epsilon\sigma_L + P_e \cdot P_p \cdot (\sqrt{1-\epsilon^2} \cdot cos\theta_\gamma \cdot A_1 \cdot \sigma_T + \sqrt{2\epsilon(1-\epsilon)} \cdot sin\theta_\gamma \cdot A_2 \cdot \sigma_T)] \quad (2)$$

where

$$A_1 = \frac{\sigma^T_{1/2} - \sigma^T_{3/2}}{\sigma^T_{1/2} + \sigma^T_{3/2}} \quad (3)$$

A_2 is a transverse-longitudinal interference term with an upper bound of

$$A_2 < \sqrt{\sigma_L/\sigma_T} \quad (4)$$

Although σ_L/σ_T is not well measured in the resonance region, it is known to be small, and is usually assumed to be of the order of 15% or less. Consequently, A_2 is expected to remain relatively small too. One can define the cross section asymmetry as:

$$A = \frac{\frac{d\sigma(+P_e)}{d\Omega_e dE'_e} - \frac{d\sigma(-P_e)}{d\Omega_e dE'_e}}{\frac{d\sigma(+P_e)}{d\Omega_e dE'_e} + \frac{d\sigma(-P_e)}{d\Omega_e dE'_e}}$$

$$= P_e \cdot P_p \cdot \frac{\sqrt{1-\epsilon^2} \cdot cos\theta_\gamma \cdot A_1 \cdot \sigma_T + \sqrt{2\epsilon \cdot (1-\epsilon)} \cdot sin\theta_\gamma \cdot A_2 \cdot \sigma_T}{\sigma_T + \epsilon\sigma_L} \qquad (5)$$

The proposed method to separate the polarization structure functions A_1 and A_2 makes use of the fact that the kinematical weighting factors in front of the respective terms have a different dependence on θ_γ and ϵ. Measurement of the asymmetry A at fixed Q^2 and W, but different beam energies, will allow a separation of the quantities of interest. In the following we discuss the sensitivity of the proposed measurement to the values of A_1 and A_2.

Measurement of A at small values of ϵ (and therefore low energies) are most sensitive to A_1, whereas intermediate values of ϵ and high energies are more sensitive to A_2. To cover a range in Q^2 and W:

$$0.2 < Q^2 < 1.5\ GeV^2, \quad 1.1 < W < 1.8\ GeV \qquad (6)$$

measurements of the asymmetry A at a variety of energies are needed.

To estimate the absolute value of the expected asymmetry and the errors in the proposed measurements we use a semi-empirical model where it is assumed that the cross section is saturated by excitation of the known baryon resonances and non-resonant single pion production as given by lowest order Born terms. This model reproduces the total photo-absorption cross section as well as differential photo- and electro-production cross sections for masses below 1.8 GeV and over a large range in Q^2 at the 10 - 20% level [BUR91]. It may therefore give some indication of how the asymmetry may depend on W and Q^2. The calculations were made for the energies, luminosities and running times as shown in Table 1.

Table 1: CLAS Operating Conditions for A1, A2 Separation		
Energy (MeV)	Luminosity ($cm^{-2}sec^{-1}$)	Run Time (hours)
1200	$2 \cdot 10^{33}$	150
1600	$2 \cdot 10^{33}$	150
2000	$3 \cdot 10^{33}$	150
2400	$5 \cdot 10^{33}$	150
2800	$5 \cdot 10^{33}$	200
3200	$1 \cdot 10^{34}$	200
4000	$1 \cdot 10^{34}$	200

We have assumed that electrons will be detected for $\theta_e = 10^0$ to 45^0 in all six sectors of CLAS.

The values of the electron and proton polarizations were taken to be $P_e = 0.5$, and $P_p = 0.9$. respectively. The choice of P_e is rather conservative, in view of recent advances in the development of strained GaAs polarized electron sources capable of producing electron beams with currents of 15-30 μA with polarization in excess of 0.75 [CAR91]. The choice of P_p is consistent with recent results. A proton polarization of 0.96 was achieved[CRA90a] using irradiated $^{15}NH_3$ as a target material in a 5T magnetic field at 1 K. This same group, using a target of similar dimensions at the Brookhaven AGS in a beam of comparable or slightly higher intensity than proposed here, achieved proton polarizations well in excess of 0.8 on a routine basis [CRA90b].

With $^{15}NH_3$ as a polarized target material, the effective polarization in inclusive scattering is given by:

$$P_p^{eff} \simeq P_p \cdot \frac{\#\text{ free protons}}{\#\text{ nucleons}} = P_p \cdot \frac{3}{18} \simeq 0.15 \qquad (7)$$

A discussion of how to establish the effective target polarization more precisely is given in section II.4

II.2 Sensitivity of A_1 to Hybrid Baryon Production

In the non-relativistic quark model (NRQM) the lowest mass $P_{11}(1440)$ state, usually called the Roper, is assigned to a radially excited 3-Quark state $[q^3]$ within the SU(6)xO(3) super-multiplet $[56,0^+]_2$ (i.e. $L_{3Q}=0$, $N_{3Q}=2$). However, the observed low mass of the state, as well as the sign and magnitude of the photocoupling amplitudes have been difficult to reproduce within the framework of the NRQM. Moreover, there is experimental evidence that the Q^2 dependence of the photocoupling amplitude $A_{1/2}(Q^2)$ may be quite different from what is predicted in the NRQM framework [LIB91]. The predictions of several different models, along with the small amount of existing data are shown in Figure 2. The data indicate a rapid fall-off of this amplitude with Q^2 whereas the NRQM and the relativized versions predict a much weaker fall-off or even a rise with Q^2. However, the experimental information about electroproduction amplitudes of the Roper is rather limited, largely due to the complete lack of polarization data, and definite conclusions about the nature of the Roper cannot be drawn from existing data.

Recently, there have been theoretical speculations [LIZ91] that the Roper resonance might not be a regular $[q^3]$ state, but the hybrid ($[q^3G]$, 3-quarks with one valence gluon) equivalent of the nucleon.

Obviously, the solution to the puzzle of the structure of the $P_{11}(1440)$ could have enormous impact on our understanding of baryon structure and the dynamics of the strong interaction in the non-perturbative regime. It has been pointed out [LIB91] that a precise measurement of the Q^2 dependence of the $\gamma_v p P_{11}(1440)$ transition form factor provides a unique means of discriminating between the interpretation of the Roper as a regular $[56,0^+]_2$ $[q^3]$ state, or as a hybrid $[70,0^+]_0$ $[q^3G]$ state. The discriminating power results from the different spin-flavor factors in the respective photocoupling amplitudes, such that in the first approximation:

$$\frac{A_{1/2}(P_{11}(1440))[70,0^+]_0}{A_{1/2}(P_{11}(1440))[56,0^+]_2} \sim \frac{1.}{Q^2} \qquad (8)$$

Therefore, the Roper is likely to fall off much more rapidly with Q^2 if it is a hybrid state than if it is a regular 3-quark state. Measurement of the Q^2 dependence of the Roper photocoupling amplitude can thus be used to discriminate

between various spectroscopic assigments. The calculation based on the hybrid interpretation is in better agreement with the data than calculations using the non-relativistic or relativized versions of the constituent quark model (Figure 2).

Measurement of the structure function $A_1(Q^2, W)$ contributes toward solving this puzzle. We first note that the $P_{11}(1440)$, being a spin 1/2 resonance, can only be excited by helicity 1/2 amplitudes ($A_{1/2}$ or $S_{1/2}$). For an isolated P_{11} resonance, the structure function $A_1 = +1$, whereas for an isolated $\Delta(1232)$, A_1 = -0.5. In both cases these values are independent of Q^2. Admixture of the tail of the P_{11} excitation tends to shift the structure function in the region of the $\Delta(1232)$ away from -0.5 towards more positive values. The value of A_1 in the Δ region is therefore a direct measure of the strength of the $P_{11}(1440)$.

To estimate the uncertainties in the determination of A_1 and A_2 a fit to the functional form (2) was made, assuming the following bins in W and Q^2:

$$\Delta W = 30\ MeV, \quad \Delta Q^2 = 0.2 \cdot Q^2 \tag{9}$$

The results are shown in Figures 3-5, where $A_1(Q^2, W)$ is shown for the q^3 and q^3G interpretations of the the Roper state. It can be noted that in the region of the $\Delta(1232)$ $A_1 \approx$ -0.5. This value is expected for the pure Δ state. Interference from the tail of the Roper makes A_1 less negative, so that the value of A_1 in this region is a clear indicator of the strength of the coupling to the Roper resonance. For these calculations, the longitudinal to transverse ratio was fixed at 0.15 throughout the resonance region. A calculation with the ratio set to 0 indicates that A_1 is rather insensitive to the choice, as seen in Figure 5.

The experimental method is relatively less accurate for measuring A_2, which is expected to be quite small and less sensitive to various model assumptions. However, a significant measurement of A_2 can be made at small Q^2 (Figure 6). A_2 is expected to be small since it depends on interference between longitudinal and transverse amplitudes. Because essentially nothing is known about the longitudinal amplitude in the resonance region, except that it is small, we do not show calculations of A_2 in Figure 6.

II.3 Q^2 Evolution of the Gerasimov-Drell-Hearn Sum Rule

The polarized proton structure function measured by the EMC collaboration [ASH88] has prompted numerous speculations about whether or not in the deep inelastic region the spin of the proton is carried by the quarks. This has led to renewed interest in experimental tests of the sum rule of Gerasimov [GER65] and Drell, Hearn [DRE66] and its Q^2 evolution. The sum rule relates the difference in the total photo-absorption cross section on nucleons for photon-nucleon helicity $\lambda_{\gamma N} = 1/2$ and $\lambda_{\gamma N} = 3/2$ to the anomalous magnetic moment of the target nucleon:

$$\int_{\nu_{th}}^{\infty} \frac{d\nu}{\nu}[\sigma_{1/2}(\nu,0) - \sigma_{3/2}(\nu,0)] = -\frac{2\pi^2\alpha}{M^2}k^2 \qquad (10)$$

where ν is the photon energy, $\sigma_{1/2}$ and $\sigma_{3/2}$ are the absorption cross sections for total helicity 1/2 and 3/2, and k is the anomalous magnetic moment of the target nucleon. The GDH sum rule has been derived on rather general grounds but has never been tested experimentally. There is evidence from the analysis of single pion production that the sum rule cannot be grossly violated [KAR73].

The interpretation of the EMC results on the polarized proton structure functions in terms of the Bjorken sum rule [BJO66] suggests [CLO88]

$$\int_{\nu_{th}}^{\infty} \frac{d\nu}{\nu}[\sigma_{1/2}(\nu,Q^2) - \sigma_{3/2}(\nu,Q^2)] \simeq \frac{0.2}{Q^2} \cdot \frac{8\pi^2\alpha}{M^2} \qquad (11)$$

The latter sum rule should be valid in the deep inelastic region. A comparison of (4) and (5) suggests that dramatic changes in the helicity structure of the γp coupling must occur when going from the deep inelastic region to $Q^2 = 0$, if the GDH sum rule were to be fulfilled. This is illustrated in Figure 7. A calculation by Anselmino et al.[ANS89], which is based on the vector meson dominance analogy shows a strong Q^2 dependence and predicts significant uncertainty resulting from the assumed effective vector meson mass. In this calculation, the GDH limit -0.535 GeV^{-2} at $Q^2 = 0$ has been used for normalization. A calculation based on the more fundamental QCD sum rules is now under way [RAD91]. Extrapolations of the photoexcitation calculations by Koniuk and Isgur [KON80], and by Close and Li [CLO90] to electroproduction are shown

as well. In addition, some semi–empirical calculations based on experimental information and single-quark-transition-model symmetry arguments are shown. Qualitatively, the change in helicity structure expected from the GDH sum rule limit and the deep inelastic EMC results is reproduced, with significant differences between the various calculations. In particular, the quark model calculations do not reproduce the GDH limit.

Figure 7 also shows the expected statistical error bars of the GDH integral $I_{GDH}(Q^2)$ for a mass cut-off at W = 1.8 GeV. Obviously, the proposed experiment will make a very significant contribution to the study of the Q^2 evolution of the sum-rule, and to our understanding of the structure of the Roper resonance.

II.4 Effect of Systematic Errors

The errors shown in Figures 3–7 are of statistical nature only. We now estimate the systematic uncertainties. We first note that untertainties in the detector efficiencies (acceptances) cancel since only count rate asymmetries for opposite electron helicities will be used in determining A_1 and A_2. Since A_1 and A_2 are not expected to exhibit very rapid changes, the experiment will also be insensitive to minor systematic shifts in the beam energy, and in the reconstructed kinematical quantities of the scattered electron. Nonetheless, we intend to make use of elastic electron-proton scattering to calibrate the detector. The following sources of systematic uncertainties are expected to yield the largest contributions to the systematic errors.

(1) Electron beam polarization

(2) Effective target polarization

Electron polarization

We propose to measure the electron polarization using Möller scattering. Möller electron polarimeters have been used in electron scattering experiments at various laboratories [COO75], [BRE85], [COA89] and the techniques are well established. The main uncertainty in the measurement of P_e is due to the limitations in measuring the magnetic flux in the thin magnetized target foil. Without any further improvement of this technique the electron polarization may be determined to $\delta P_e/P_e \simeq 0.05$.

Target polarization

The uncertainty in the knowledge of the target polarization is comparable to that in the beam polarization. A direct measurement of the polarization has an absolute accuracy of about $\pm$ 3%. In addition to this uncertainty, the proposed target material $^{15}NH_3$ has the disadvantage versus alcohol based materials (such as butanol doped with chemical radicals) in that the unpaired proton in the nitrogen nucleus will, to some degree, be polarized. The polarization is known to be about 16% for a 90% polarization of the free proton. However, since the dilution factor is 3 times larger, the effective contribution of the nitrogen polarization is

$$P^{eff}_{^{15}N} = P_{^{15}N} \cdot \frac{\#\text{ polarized protons in } ^{15}N}{\#\text{ nucleons in } ^{15}NH_3} \simeq 0.009 \qquad (12),$$

assuming equal contributions from all nucleons in the ^{15}N nucleus. This corresponds to about 6% of the effective free proton polarization. The relevant contribution to the inelastic asymmetry will be from quasifree scattering off the unpaired proton in the ^{15}N. Using realistic ^{15}N wavefunctions, we expect that the correction factor may be calculated with an uncertainty of less than 30%, which reduces the systematic uncertainty in the asymmetry to less than 2%. We also note that the correction is an overall multiplicative factor, which may be adjusted as more accurate theoretical calculations become available.

In addition, we propose a method that will allow a more direct measurement of the effective target polarization. This method is outlined in the following section.

Determination of the product of beam and target polarization

We propose to measure the product $P_e \cdot P_p$ in elastic electron scattering off free protons and in quasi-elastic scattering off bound protons. Using the good missing mass resolution of CLAS, elastic and quasi-elastic processes can be separated. A simulation of the two processes for a typical kinematical situation is shown in Figure 8. The CLAS detector will record elastic $\vec{p}(\vec{e},e')p$, and quasi-elastic $^{15}\vec{N}(\vec{e},e')X$ events in parallel with the inelastic events. We therefore propose to use the same technique to extract the asymmetry A^{ep} for elastic and quasi-elastic scattering. For elastic scattering of a polarized electron from a free polarized proton the asymmetry is given by [DON86]

$$A^{ep} = A_1 \cos\theta_\gamma + A_2 \sin\theta_\gamma \qquad (13)$$

where

$$A_1 = \frac{2\tau v'_T}{v_L(1+\tau)\cdot(G_E^p/G_M^p)^2 + 2\tau v_T} \tag{14}$$

and

$$A_2 = \frac{2\sqrt{2\tau(1+\tau)}\cdot(G_E^p/G_M^p)v'_{TL}}{v_L(1+\tau)\cdot(G_E^p/G_M^p)^2 + 2\tau v_T} \tag{15}$$

where

$$\tau = \frac{Q^2}{4M_p^2}$$

$$v_L = (\frac{Q^2}{q^2})^2$$

$$v_T = \frac{Q^2}{2q^2} + \tan^2\frac{\theta}{2}$$

$$v'_T = \tan\frac{\theta}{2}\sqrt{\tan^2\frac{\theta}{2} + \frac{Q^2}{q^2}}$$

$$v'_{TL} = -\frac{Q^2}{q^2}\frac{\tan\frac{\theta}{2}}{\sqrt{2}}$$

Here $q^2 = Q^2 + \nu^2$ is the conventional notation. Since G_E^p and G_M^p are accurately known at small Q^2, measurement of the experimental asymmetry

$$A^{exp} = P_e \cdot P_p \cdot A^{ep} \tag{16}$$

allows the extraction of the product of beam and target polarization. The same techniques can be used to measure the product of beam polarization and effective ^{15}N polarization. The elastic ep asymmetry is shown in Figure 9 along with the expected statistical errors using the running times proposed for this experiment. In these calculations a conservative estimate of 2% was used for the experimental uncertainties in the form factors. Besides the statistical uncertainties, the main contribution to the uncertainty is due to the uncertainty in the measurement of Q^2. Since measurements of the same factor can be made in many Q^2 bins at each energy, the statistical uncertainty can be significantly reduced, leaving an uncertainty of less than .01 in P_eP_p. This is a substantial improvement over the direct measurements of the polarizations.

Correction for scattering on ^{15}N

The experimentally measured asymmetry is given by:

$$A_1^{exp} = P_e \cdot \frac{3 \cdot (\sigma_{1/2}^T - \sigma_{3/2}^T) \cdot P_P + ("\sigma_{1/2}^T" - "\sigma_{3/2}^T") \cdot "P_P"}{6 \cdot (\sigma_T + \epsilon\sigma_L) + 2\sigma_{TOT}(^{15}N)},$$

where "$\sigma_{1/2}^T$" denotes the helicity 1/2 quasi-free cross section on ^{15}N.

The demoninator contains the total cross section for scattering on the ^{15}N nucleus. For a precise measurement of this contribution, the polarized target material will be replaced by a ^{15}N target under otherwise identical condition (target geometry, polarized target field, beam rastering, etc.). The two measurements will be normalized to each other by matching the areas under the quasi-elastic peak in the missing mass regions outside of the elastic ep scattering peak. (Figure 9).

III. Performance of the CLAS Detector with Polarized Target Field.

The axial field component B_z of the polarized target is shown in Figure 10 as a function of r and z. For a central magnetic field of 5 Tesla one obtains $\int$Bdl = 1.0Tm. Deflection of charged particles in the target field might therefore seriously affect the acceptance of charged particles in CLAS. Clearly, the largest deflection will occur for particles emitted at 90° with respect to the symmetry axis of the target field. Charged particle trajectories with momenta between 150 MeV/c and 2000 MeV/c are displayed in Figure 11. The polarized target magnetic field strongly deflects low momentum particles, resulting in an effective low momentum cut-off at $\approx$ 150 MeV/c. Except for this cut-off, the CLAS acceptance for single particles is only slightly affected if one ignores the fact that the ϕ acceptance is shifted by an angle $\Delta\phi(p)$. The analysis of the trajectories is facilitated by the fact that the particle trajectories after leaving the polarized target field region still appear to be pointing back to the emission point at the target. Momentum resolution for reconstructed trajectories is, to first order, not affected by the presence of the target magnetic field, since most of its $\int$Bdl is concentrated inside the region where the CLAS tracking chambers are located. Similarly, the resolution in the polar and azimuthal scattering angle is not affected by the presence of the target field, assuming the target field distribution is known with sufficient precision.

IV.1 Beam Handling in Polarized Target Operation.

In most applications of polarized targets pertaining to the study of nucleon resonance excitation, the polarization vector is aligned parallel to the direction of the incident electron beam. In this configuration the primary beam is unaffected, except for the (minor) focussing properties of the target field.

Beam rastering.

The polarizability of the protons and deuterons in $^{15}NH_3$ strongly depends upon its exposure to ionizing particle beams. In fact, the material must be pre-irradiated with about 10^{17} particles per cm^2 to reach its optimum performance. In case of a physics experiment, the polarization degree can change (increase or decrease) depending on the history of the target sample. To avoid local depolarization or polarization buildup, due to non-uniform exposure of the target sample to the beam, the incident beam will be rastered across the target front face. To avoid local temperature rise within the target sample, high speed beam rastering is necessary. This can be achieved by incorporating four small dipole magnets, made of laminated magnetic steel, upstream in the beam line.

IV.2 Background and Luminosity Issues for Polarized Target Operation.

Since a polarized solid state target has a strong magnetic field associated with it, the trajectories of charged background particles coming from the target region will be strongly influenced by the field orientation chosen for a specific experiment. Background events have been simulated using the GEANT3 [BRU86] package, and a realistic event generator. The event generator was based on events generated using the EGS4 package corrected for wide angle bremsstrahlung, and X-ray production.

The target sample used in the simulation is in the shape of a cylinder of 1.5 cm length and 1 cm radius.

With the target polarized along the beam direction, the longitudinal magnetic field of the target acts like a focussing lens, and keeps practically all low energy charged particles emerging from the target within a narrow cone surrounding the beam axis, even those emitted at large angles to the beam. This effect is illustrated in Figure 13. This shielding of low energy particles from the CLAS tracking volume is at least as effective as the shielding obtained with the

standard miniature torus. The wire chambers appear to be nearly unaffected by charged background. Therefore, we can expect the CLAS detector to safely operate at luminosities of 10^{34} $cm^{-2}sec^{-1}$ (and possibly beyond) in conjunction with a polarized target having the polarization axis aligned along the beam axis.

Note that the simulations were done with the CLAS configuration as outlined in the Preliminary Conceptual Design Report [CLA89]. However, we do not expect any significant change in the background situation for the current detector geometries.

IV.3 Mechanical Aspects of Polarized Target Operation in CLAS.

The mechanical support structure has to serve two functions; it holds the target magnet in place, and it has to carry the magnetic forces resulting from the interference of the target field with the main torus field. Also, it should not obstruct any additional solid angle. The present design makes use of a rigid connection of the magnet cryostat to the torus cryostat in the rear. The layout of the target magnet, the target cryostat, and the support structure in the CLAS magnet as currently envisioned are shown in Figure 13. As illustrated in Figure 14, the polarized target magnet coils will be placed in a their own cryostat, which is separated from the polarized target cryostat, providing more flexibility in servicing the target as well as in changing the orientation of the magnetic field.

V. Summary of Beam Requests and Equipment Requirements

Our request for running time, beam energies, approximate currents, and targets is summarized in table 2. The quoted numbers do not include time needed for servicing the polarized target, such as annealing, refilling liquid helium dewars, etc. All measurements will be conducted using the polarized electron source. We assume that the CLAS detector will be fully instrumented with tracking chambers, gas Cerenkov counters, scintillation counters, and electromagnetic calorimeters for angles up to 45°. Estimated running times are given for two values of the beam polarization. The running time is approximately proportional to $1/P_e^2$.

Total amount of beam time requested ($P_e = 0.5$):

1,200 hours of running with polarized $^{15}NH_3$ target

120 hours of unpolarized running with ^{15}N target

Total amount of beam time requested ($P_e = 0.75$):

530 hours of running with polarized $^{15}NH_3$ target

58 hours of unpolarized running with ^{15}N target

VI. Responsibilities

CEBAF and the University of Virginia are jointly responsible for the polarized target magnet. The University of Virginia will design and build the polarized target cryostat with the assistance of the CEBAF engineering group. The University of Virginia will be responsible for the operation of the polarized target. Data will be analyzed jointly by CEBAF, U.Va. and other members of the collaboration.

Table 2: CEBAF Operating Conditions for A1, A2 Separation				
Energy (MeV)	Target	Current (nA)	Running Time (hours)	Running Time (P_e=0.75)
1200	$^{15}NH_3$	1	150	65
1200	^{15}N	1	15	7
1600	$^{15}NH_3$	1	150	65
1600	^{15}N	1	15	7
2000	$^{15}NH_3$	1.5	150	65
2000	^{15}N	1.5	15	7
2400	$^{15}NH_3$	2.5	150	65
2400	^{15}N	2.5	15	7
2800	$^{15}NH_3$	2.5	200	90
2800	^{15}N	2.5	20	10
3200	$^{15}NH_3$	5	200	90
3200	^{15}N	5	20	10
4000	$^{15}NH_3$	5	200	90
4000	^{15}N	5	20	10
TOTAL	$^{15}NH_3$		1,200	120
TOTAL	^{15}N		530	58

References

[ANS89] M. Anselmino, B.L. Ioffe, E. Leader, Yad. Fiz.**49**, 214 (1989), transl. in Sov. J. Nucl. Phys. **49**, 136 (1989).

[ARR91] J. Arrington *et al.*; CALTECH Preprint OAP-711 (1991)

[ASH88] J. Ashman *et al.*, Phys. Lett.**206B**,364 (1988).

[BAU80] G. Baum *et al.*, Phys. Rev. Lett.**45**, 2000 (1980); R.F. Oppenheim et al. SLAC-PUB 3026 (1982)

[BJO66] J.D. Bjorken, Phys. Rev.**148**, 1467 (1966)

[BOD] B. Boden and G. Kroesen, Research Program at CEBAF II, Report of th 1986 Summer Study Group, eds. V. Burkert et al., Newport News, VA 23606, USA, and private communications.

[BRE85] W. Brefeld *et al.*, Nucl. Instr. Meth.**228**, 228 (1985)

[BRU86] R. Brun et al.; GEANT3, CERN DD/EE/84-1 (1986)

[BUR91] V. Burkert; A_AND_O - Code, unpublished.

[CAR91] L. Cardman; Talk presented at the conference on Intersection between Particle and Nuclear Physics, Tucson, Arizona, May 24 - 29, 1991.

[CLO78] F.E. Close, Introduction To Quarks and Partons (Academic Press, New York) (1979).

[CLO88] F.E. Close; Proc. Workshop on 'Excited Baryons 88', Troy, NY, 4 - 6 August, 1988, eds. G. Adams et al, publ. World Scientific.

[CLO90] F.E. Close and Z.P. Li, Phys. Rev.**D42**,2194 (1990)

[COO75] P.S. Cooper, *et al.*, Phys. Lett.**34**, 1589 (1975)

[COA89] G.D. Coates *et. al*, NIM in Phys. Res.**A278**,293 (1989).

[CRA90a] D. G. Crabb *et. al*, Phys. Rev. Lett.**64**,2627 (1990).

[CRA90b] D. G. Crabb; Talk presented at the Workshop on Polarized Solid Target, Bonn, Germany, 7-8 Sept. 1990.

[DON86] T.W. Donnelly and A.S. Raskin, Annals of Physics**169**, 247 (1986)

[DRE66] S.D. Drell and A.C. Hearn, Phys. Rev. Lett.**16**, 908 (1966).

[FOS82] F. Foster and G. Hughes, Z. Phys.**C14**,123 (1982).

[GER65] S. Gerasimov, Yad. Fiz. (1965), Soviet J. Nucl. Phys.**2**, 930 (1966)

[GER80] C. Gerhardt, Z. Phys**C4**, 311 (1980).

[KAR73] I. Karliner, Phys. Rev., **D7**, 2717 (1973)

[KON80] R. Koniuk and N. Isgur, Phys. Rev. **D21**, 1888(1980).

[LIB91] Z.P. Li, V. Burkert, Z. Li; CEBAF Preprint PR-91-032 (1991)

[LIZ91] Z.P. Li; University of Tennessee preprint, UTK-91-05, to be published in Phys. Rev.**D**

[MEY85] W. Meyer; 1985 CEBAF Summer Workshop, pg 237.

[NEL85] W.R. Nelson; The EGS4 Code System, SLAC Report 265 (1985)

[PCD88] CEBAF Preconceptual Design Report for Experimental Equipment (1988)

[RAD91] A. Radyushkin; private communication

[WEB90] H.J. Weber, Phys. Rev.**C41**, 2783 (1990).

[WPT84] Proceedings 4^{th} International Workshop on Polarized Target Materials and Techniques, Bad Honnef, September 1984.

Figure Captions

Figure 1. (a) A diagram of the electron scattering for arbitrary orientation of the nucleon polarization, $\vec{P}_p$. $\vec{q}$ makes an angle θ_γ with the initial electron beam. The angles ψ and ϕ are the polar and azimuthal angles of the polarization vector with respect to $\vec{q}$ and the electron scattering plane.

(b) Electron scattering with $\vec{P}_p$ oriented along the electron beam.

Figure 2. The structure function, $A_{1/2}$ as a function of Q^2. The points with error bars show model dependent extractions from data. The open diamonds are the results of a fit at fixed Q^2 by G. Gerhardt [GER80]. The two lines ending at Q^2 =1 are different results of an analysis by Gerhardt, constrained by a photoproduction value of $A^P_{\frac{1}{2}}(0) = -50{\cdot}10^{-3}$ GeV$^{-1/2}$. The other points are from an analysis of Boden and Kroesen [BOD86], also at fixed Q^2. The upper line (dashed) and the dash-dot line are calculations of Weber[WEB90] using a relativistic quark model, with configuration mixing. The dash-dot-dot line is from Foster and Hughes [FOS82]. The lines that remain negative are as follows: the solid line is from the empirical calculation described in the proposal. The lowest line (dashed) is a calculation treating the Roper as a 3q state, and the dash-dot line above this one uses a hybrid model [LIB91].

Figure 3. Calculations of $A_1(Q^2, W)$ at $Q^2 = 0.25$ GeV^2 and $Q^2 = 0.75$ GeV^2 using the program described in the text. The ratio σ_L/σ_T was fixed at 0.15. The dashed line shows the result with the assumption that the Roper is a q^3 state and the solid line shows the result if it is assumed to be a hybrid q^3G state. The Roper width was taken to be Γ = 150 MeV. The error bars show the expected measurement errors in $A_1(Q^2, W)$ for the proposed experiment.

Figure 4. Same as Figure 3, except that Q^2 = 1.0 GeV^2 and 1.5 GeV^2. The points with error bars are from SLAC data [BAU80].

Figure 5. The upper graph is the same as for Figure 3, except that Q^2 = 2.0 GeV^2. In the lower graph, the effect of the choice for the ratio, σ_L/σ_t is shown. The solid line uses 0.15 and the dotted line uses 0 for the ratio. In addition the dashed curve was obtained by systematically increasing the asymmetry measurement at 2.0 GeV by 2%.

Figure 6. Estimated accuracy for the measurement of $A_2(Q^2, W)$ at (a) Q^2

= 0.25 GeV^2, and (b) Q^2 = 1.00 GeV^2. Since A_2 depends on the interference between longitudinal and transverse amplitudes, not enough is known about the ratio of the two throughout the resonance region to make a sensible calculation.

Figure 7. The Gerasimov-Drell-Hearn integral as a function of Q^2 for different models. The line labeled GDH SR shows the value of the GDH sum rule (Q^2 = 0). The two lines around -0.58 at Q^2 = 0., were obtained with the semi-empirical calculation described in this proposal: the solid line obtained with Roper treated as a gluonic hybrid, and the dashed line with it treated as a 3-quark object. The dash-dot-dot line starting at the GDH sum rule uses the form of Anselmino et al. [ANS89], with the vector meson mass scale equal to the m_ρ. The two curves that start around 0 at Q^2 = 0 are obtained by extrapolating the model of Close and Li [CLO90](solid line) and the model of Koniuk and Isgur [KON80] (dashed line) from photoproduction. The solid line that extrapolates to large positive values at Q^2 = 0, is a line fit with a $1/Q^2$ dependence to the EMC measurements at higher Q^2. The figure also shows the expected statistical error bars of the GDH integral for a mass cut-off at $W = 1.8\ GeV$.

Figure 8. Results of a simulation of the elastic and quasi-elastic electron scattering processes in the CLAS for a typical kinematical situation, showing the narrow elastic peak riding on a much broader quasielastic peak.

Figure 9. (a) The asymmetry for elastic electron scattering for various values of Q^2 and incident energies. (b)The expected errors in the product of the beam polarization, P_e, and the effective ^{15}N polarization, at several values of Q^2 and the proposed incident energies. The errors were calculated by assuming ΔQ^2 = 0.1 Q^2. (c) The expected error in the measurements when the statistical error is negligible.

Figure 10. The radial and axial distribution of B_z of the split pair coil arrangement.

Figure 11. Charged particle trajectories through the target magnet and through the CLAS torus, for momenta of 150, 250, 500, 1000, 1500, and 2000 MeV/c.

Figure 12. Charged particle background when the field axis is aligned with the beam direction.

Figure 13. Layout of the polarized target magnet, the target cryostat, and the support structure in the CLAS magnet.

Figure 14. Superconducting split pair magnet with the coil shape designed for minimal solid angle obstruction and maximum field homogeneity. The magnet coils are placed in a their own cryostat, separated from the polarized target cryostat.

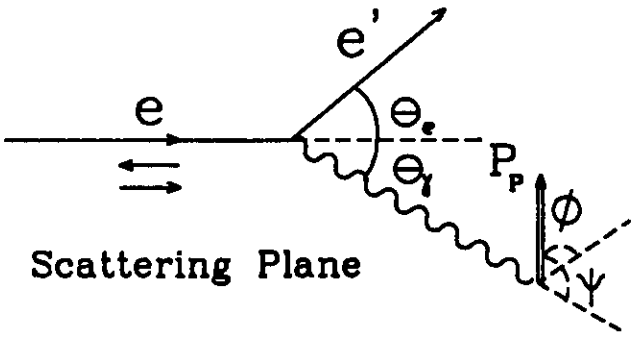

Figure 1a

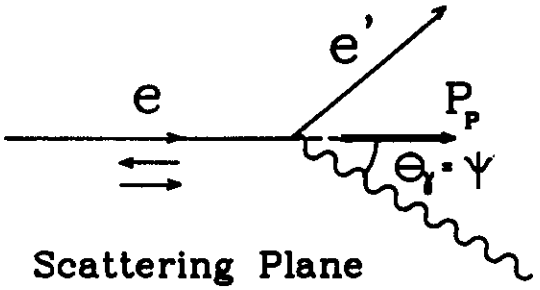

Figure 1b

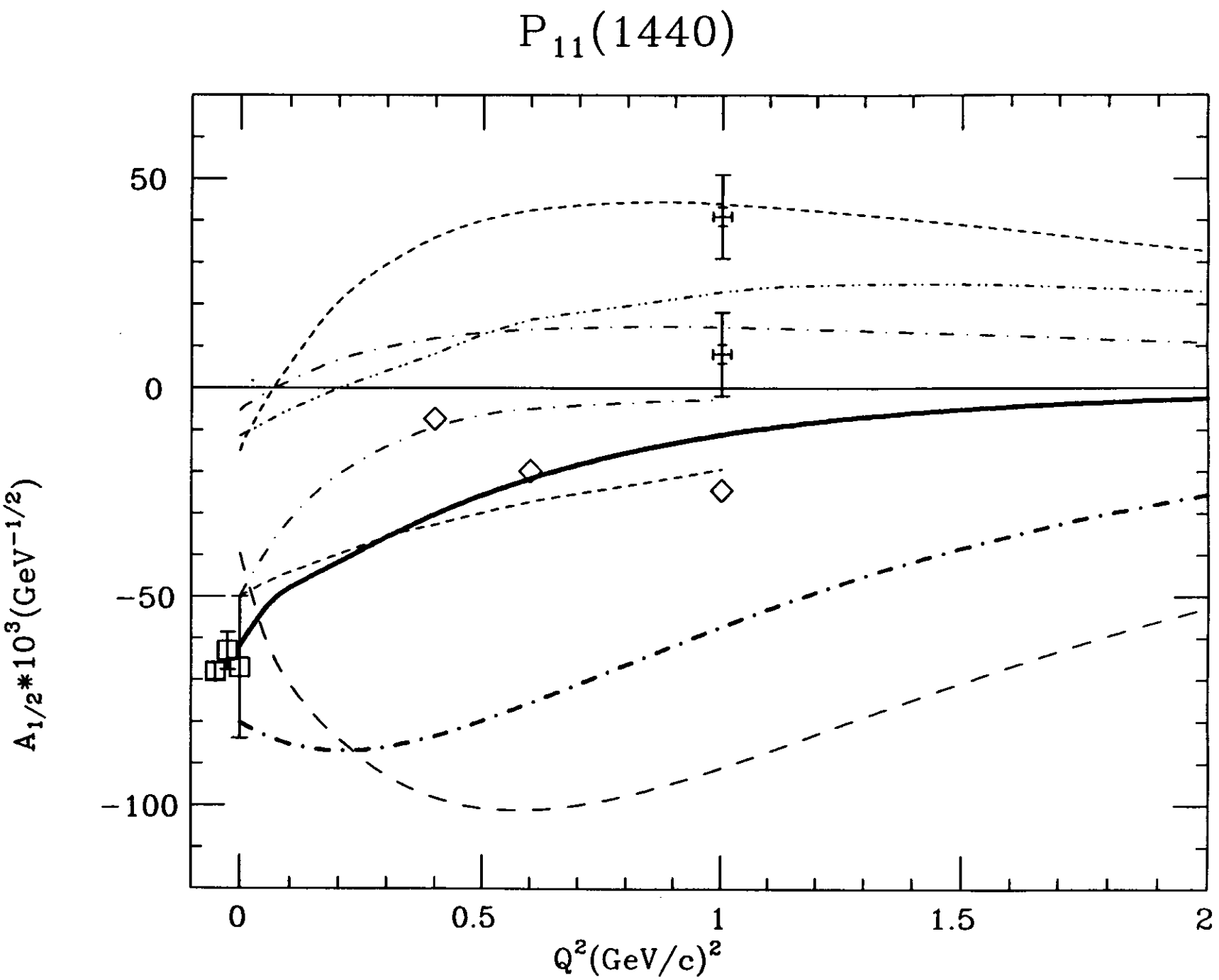

Figure 2

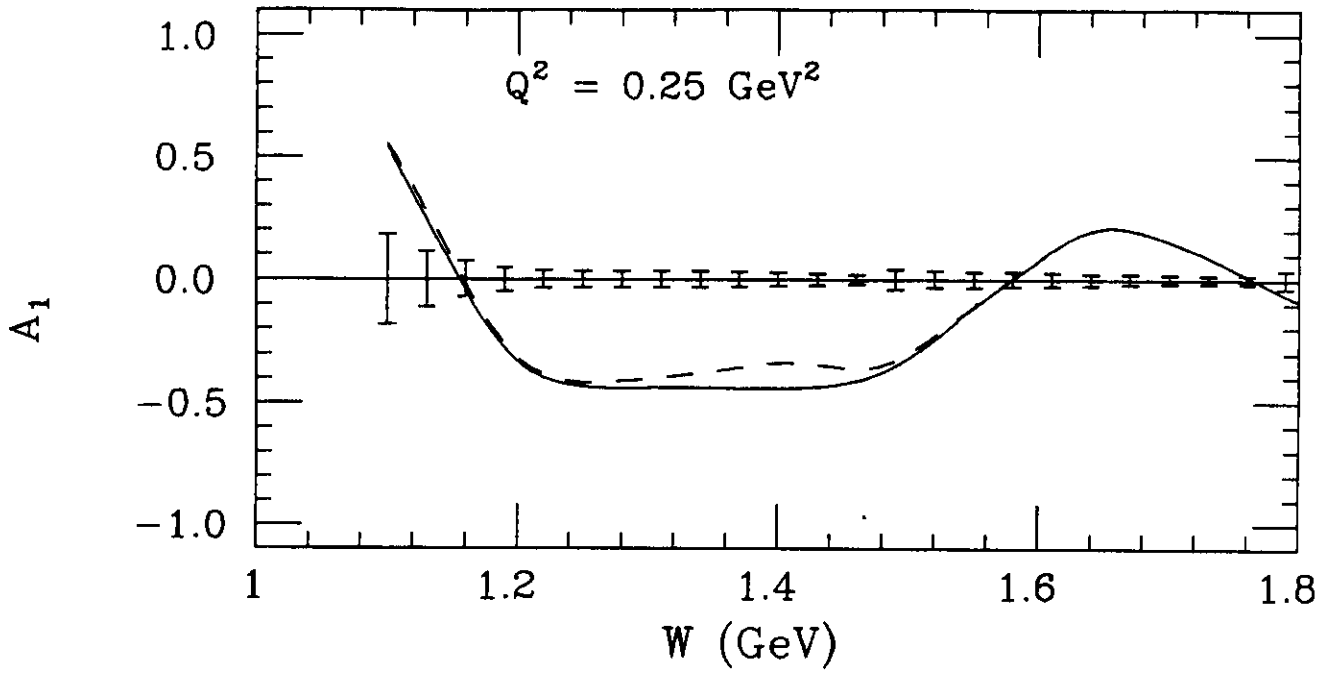
Q^2 = 0.25 GeV^2
A_1
1.0
0.5
0.0
−0.5
−1.0
1
1.2
1.4
1.6
1.8
W (GeV)

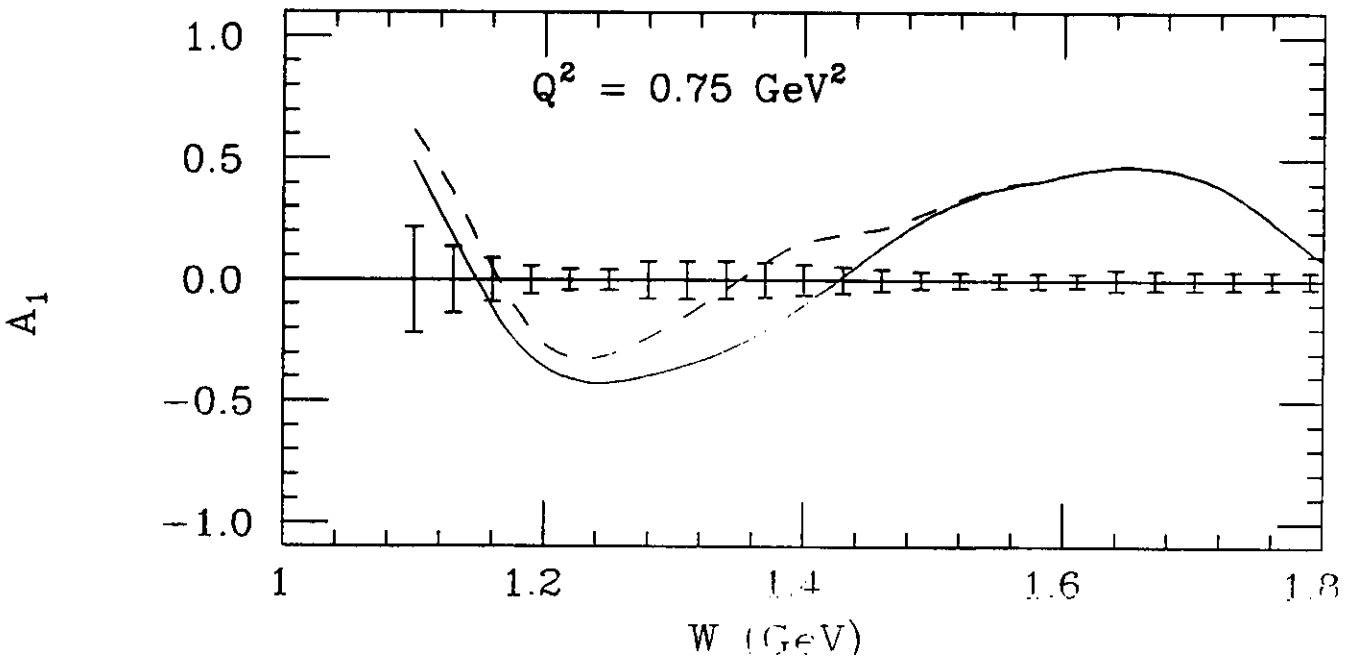
Q^2 = 0.75 GeV^2
A_1
1.0
0.5
0.0
−0.5
−1.0
1
1.2
1.4
1.6
1.8
W (GeV)

Figure 3

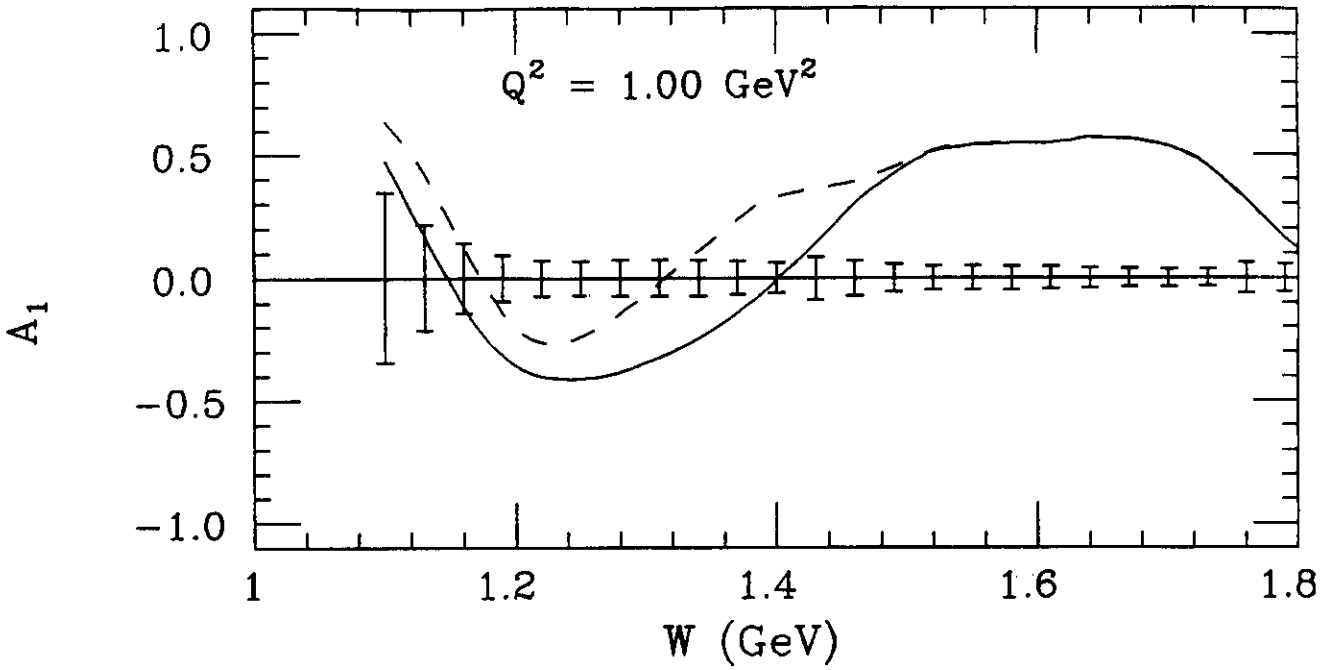
Q^2 = 1.00 GeV^2
A_1
1.0
0.5
0.0
−0.5
−1.0
1
1.2
1.4
1.6
1.8
W (GeV)

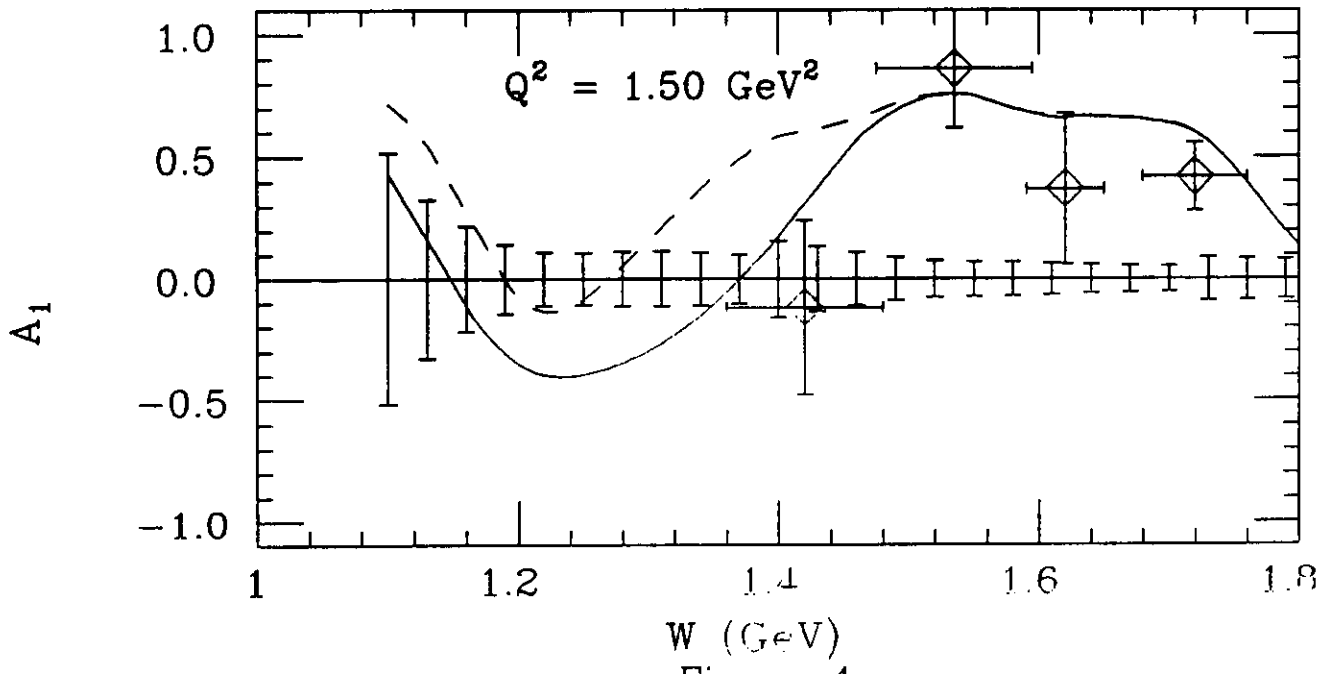
Q^2 = 1.50 GeV^2
A_1
1.0
0.5
0.0
−0.5
−1.0
1
1.2
1.4
1.6
1.8
W (GeV)

Figure 4

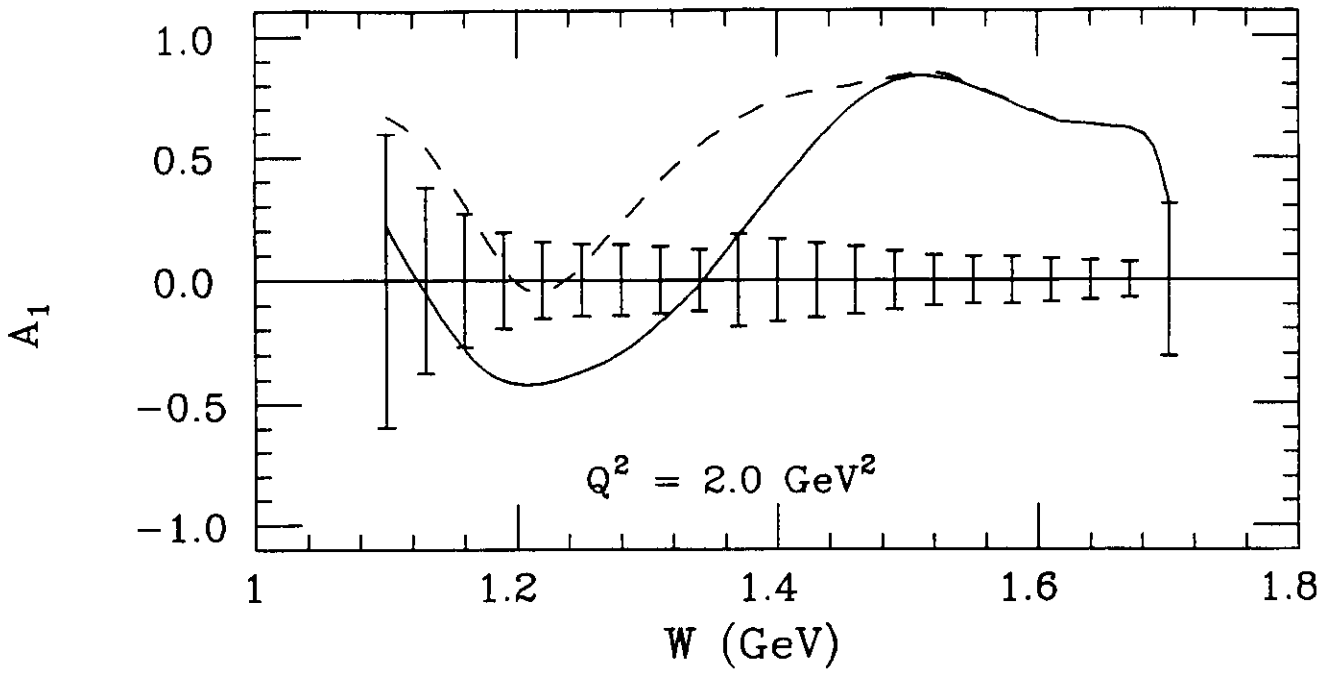
1.0
0.5
0.0
−0.5
−1.0
A1
Q2 = 2.0 GeV2
1
1.2
1.4
1.6
1.8
W (GeV)

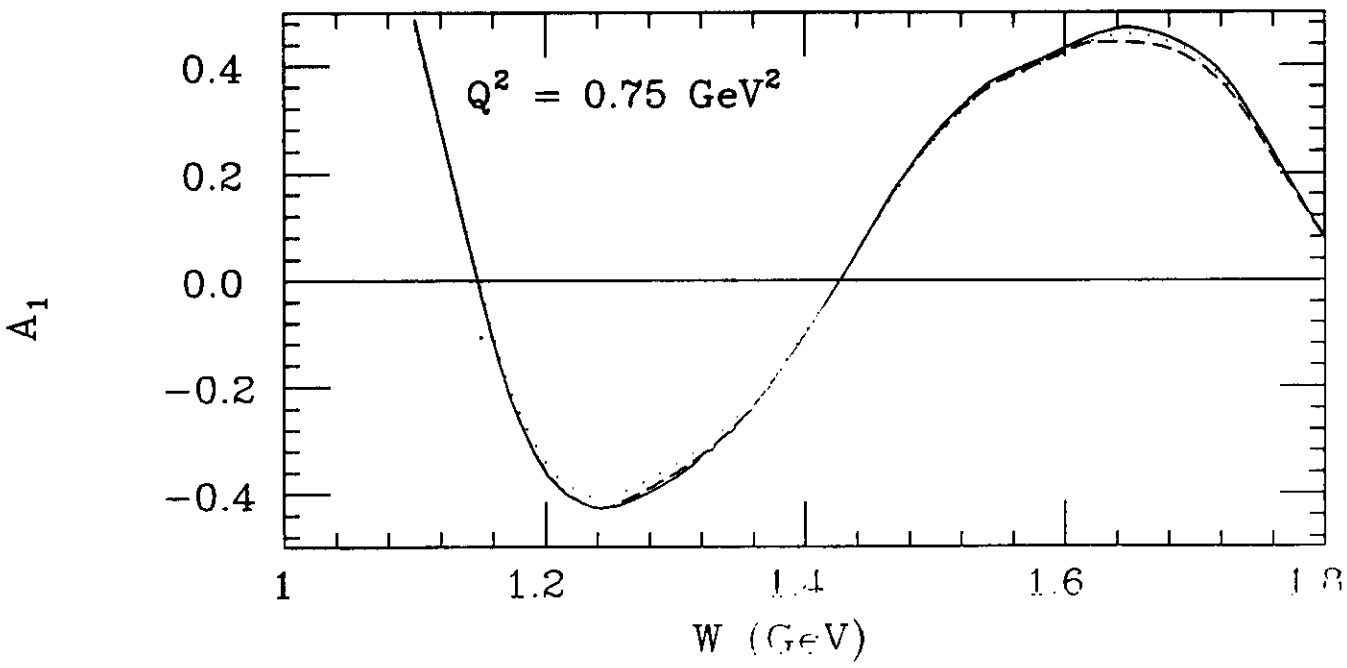
0.4
0.2
0.0
−0.2
−0.4
A1
Q2 = 0.75 GeV2
1
1.2
1.4
1.6
W (GeV)

Figure 5

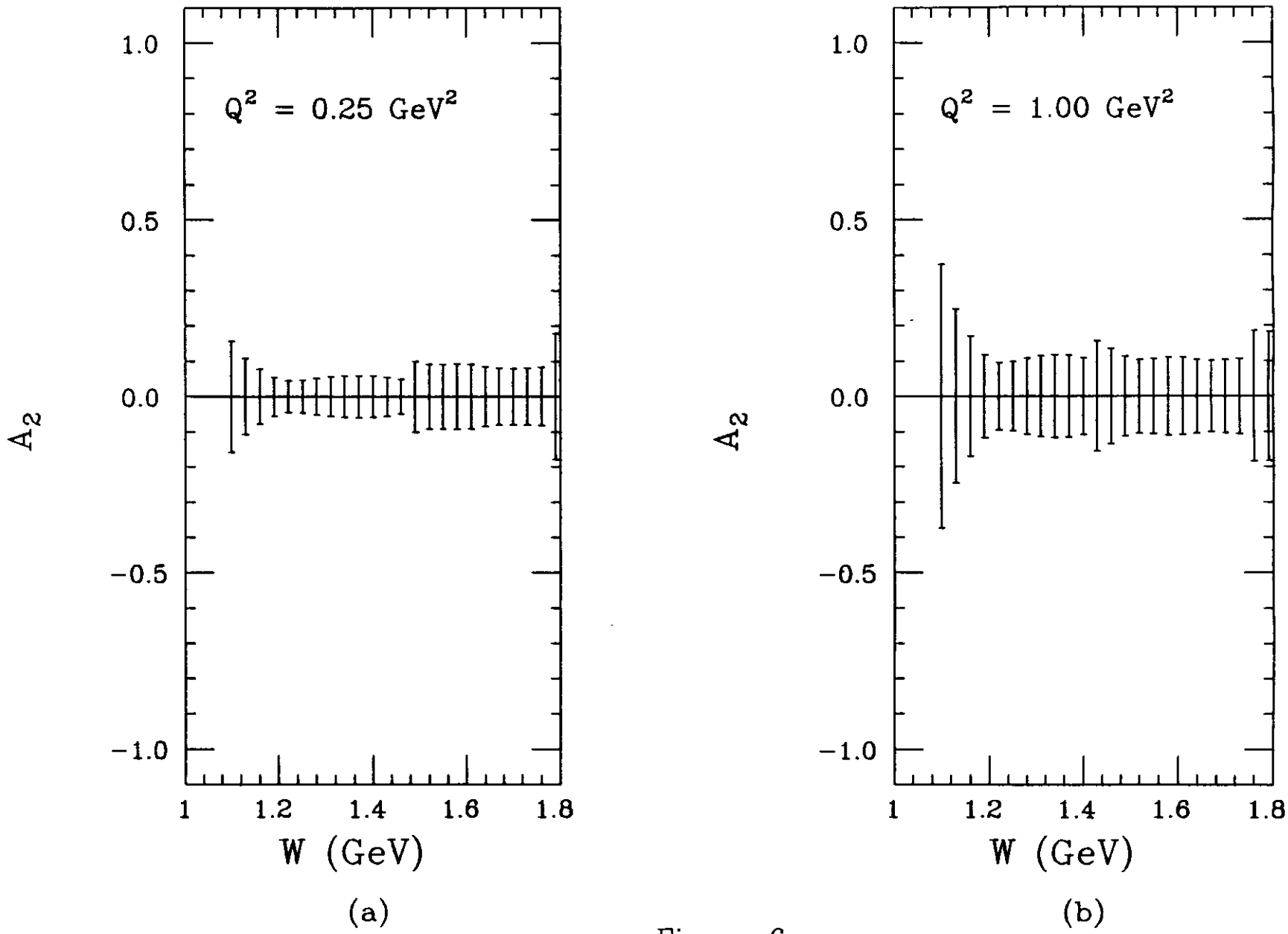
1.0
0.5
0.0
−0.5
−1.0
A_2
Q^2 = 0.25 GeV^2
1
1.2
1.4
1.6
1.8
W (GeV)
(a)
1.0
0.5
0.0
−0.5
−1.0
A_2
Q^2 = 1.00 GeV^2
1
1.2
1.4
1.6
1.8
W (GeV)
(b)

Figure 6

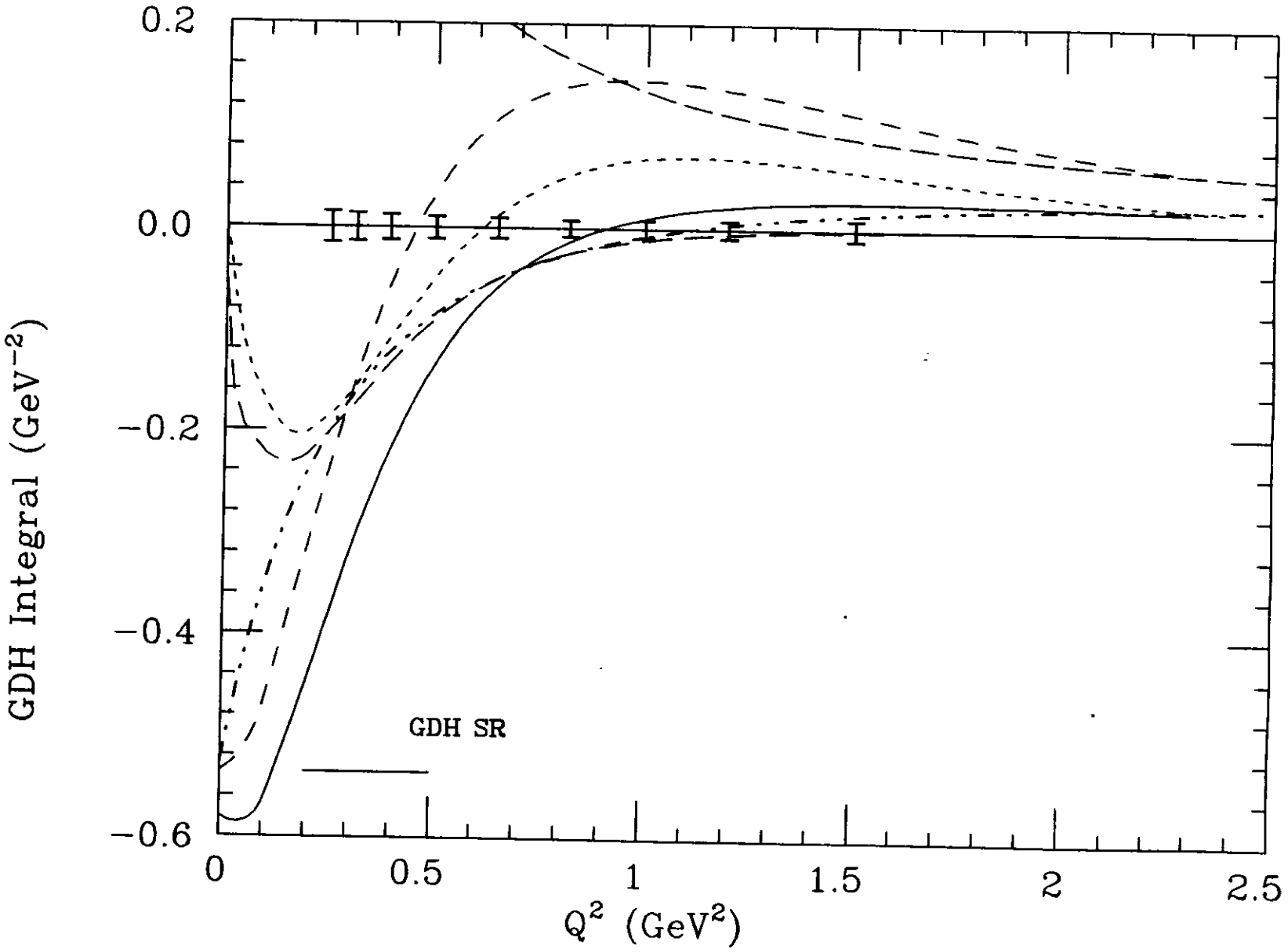

Figure 7

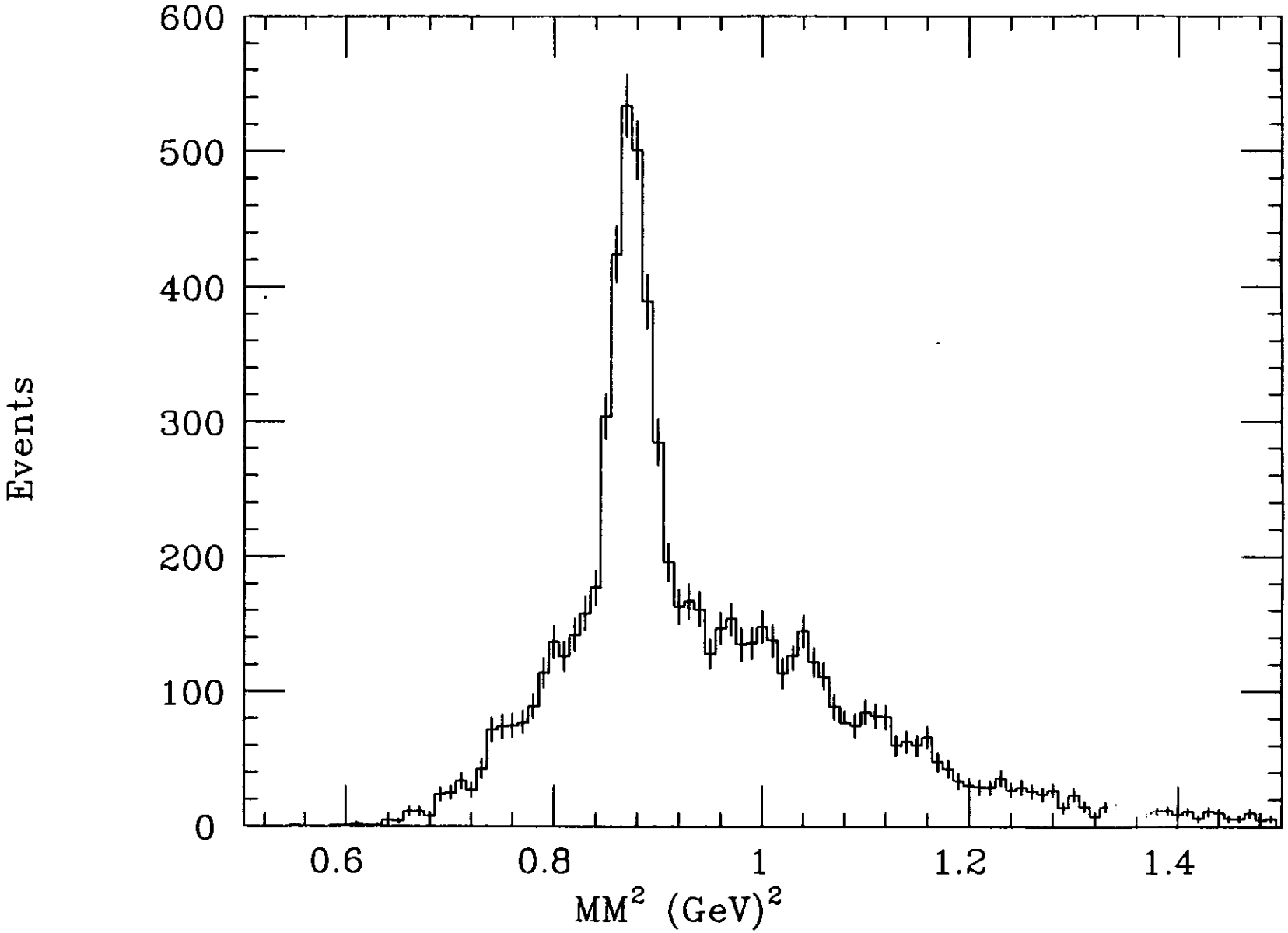

Figure 8

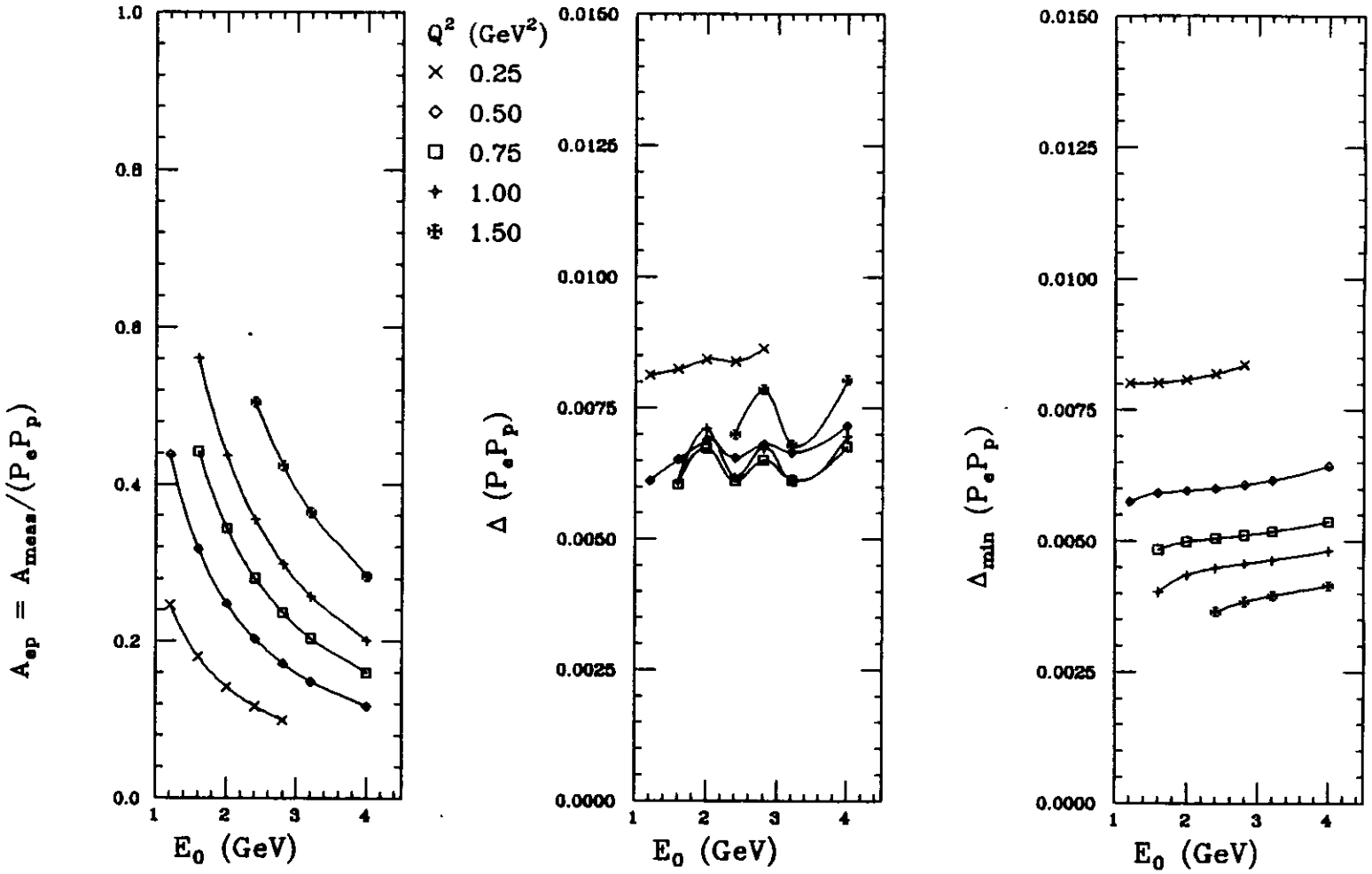
$A_{ep} = A_{meas}/(P_e P_p)$
Q^2 (GeV^2)
0.25
0.50
0.75
1.00
1.50
E_0 (GeV)
(a)
Δ ($P_e P_p$)
E_0 (GeV)
(b)
Δ_{min} ($P_e P_p$)
E_0 (GeV)
(c)

Figure 9

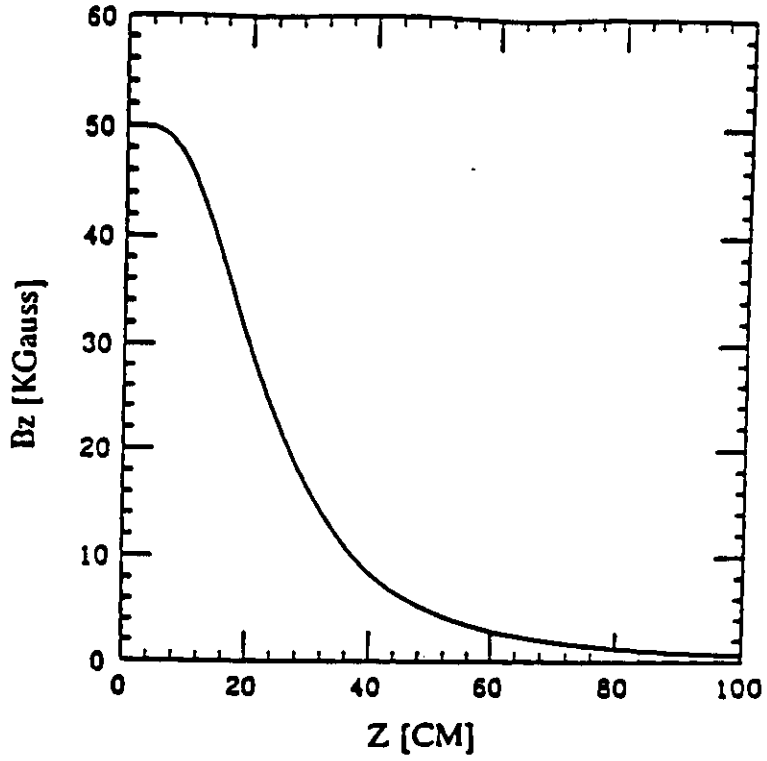
60
50
40
30
20
10
0
Bz [KGauss]
0
20
40
60
80
100
Z [CM]

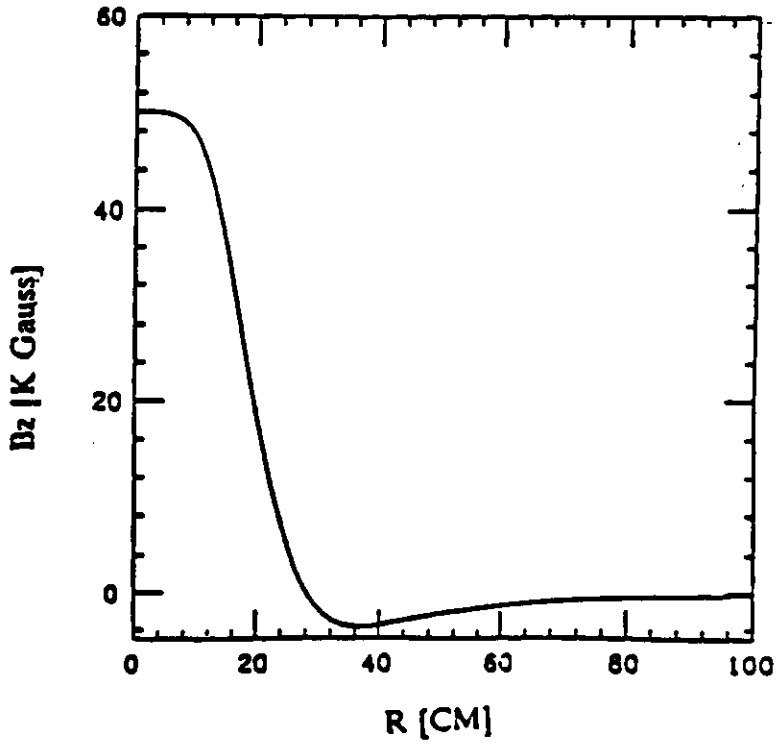
60
40
20
0
Bz [K Gauss]
0
20
40
60
80
100
R [CM]

Figure 10

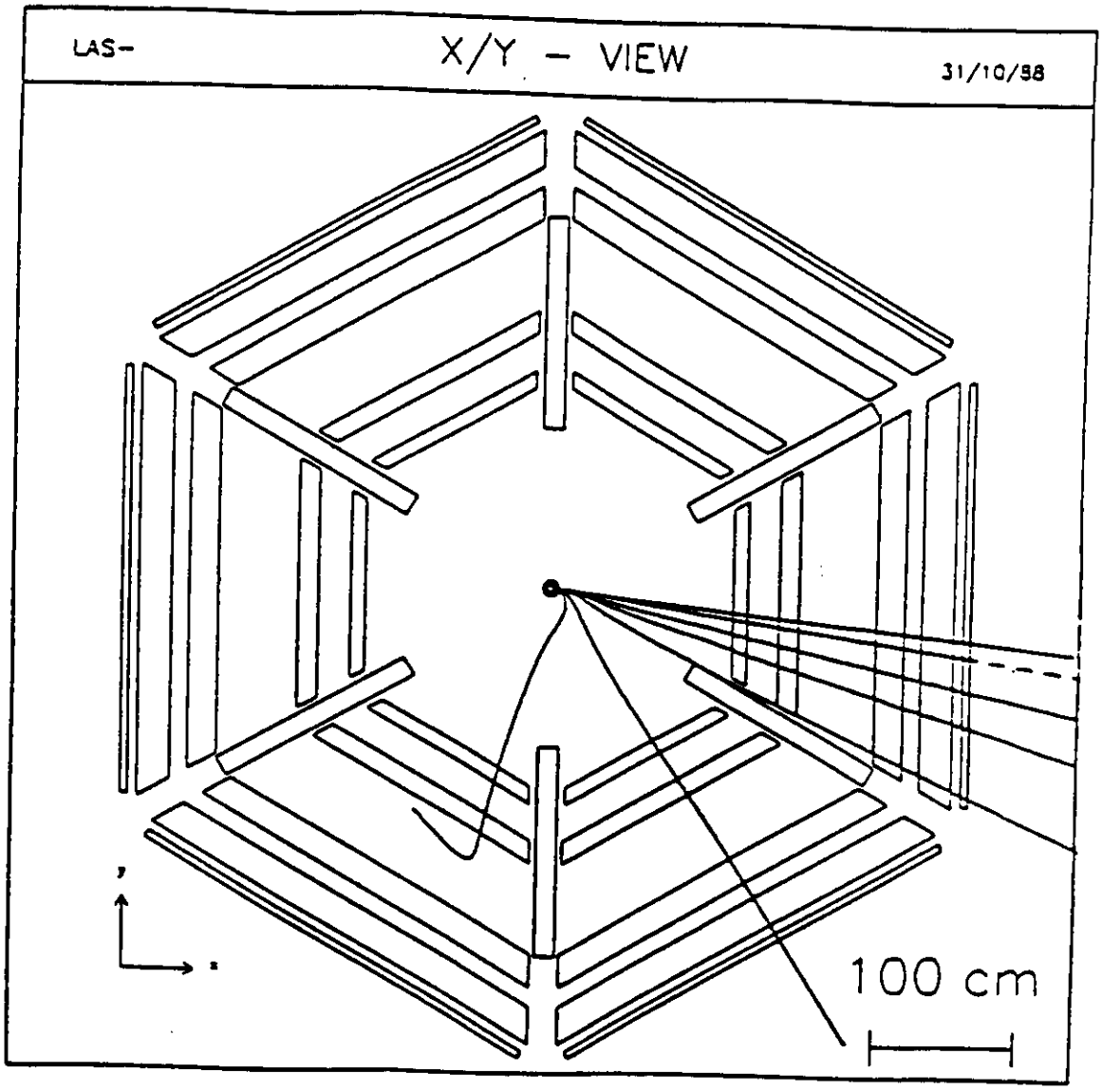

Figure 11

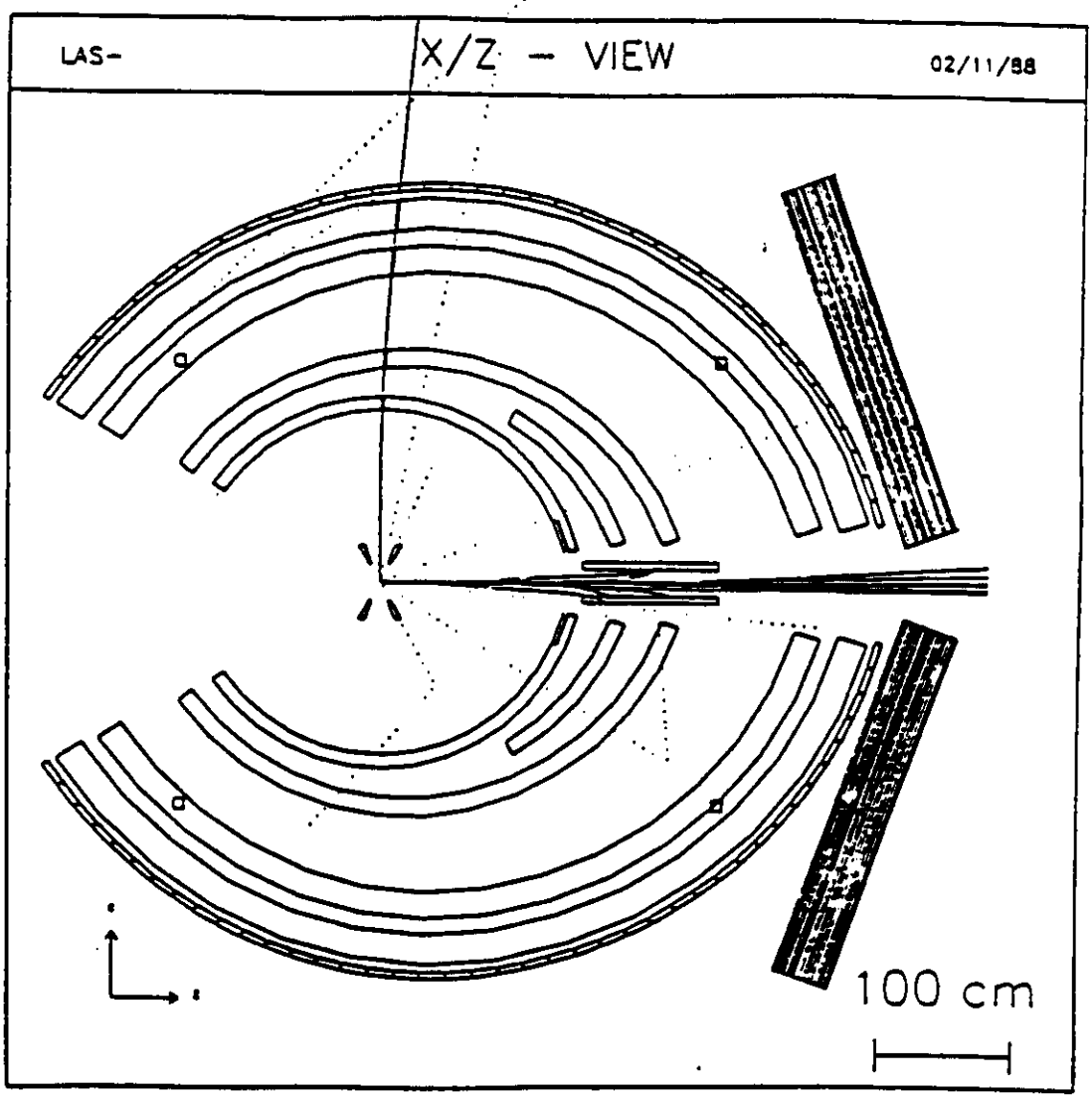

Figure 12

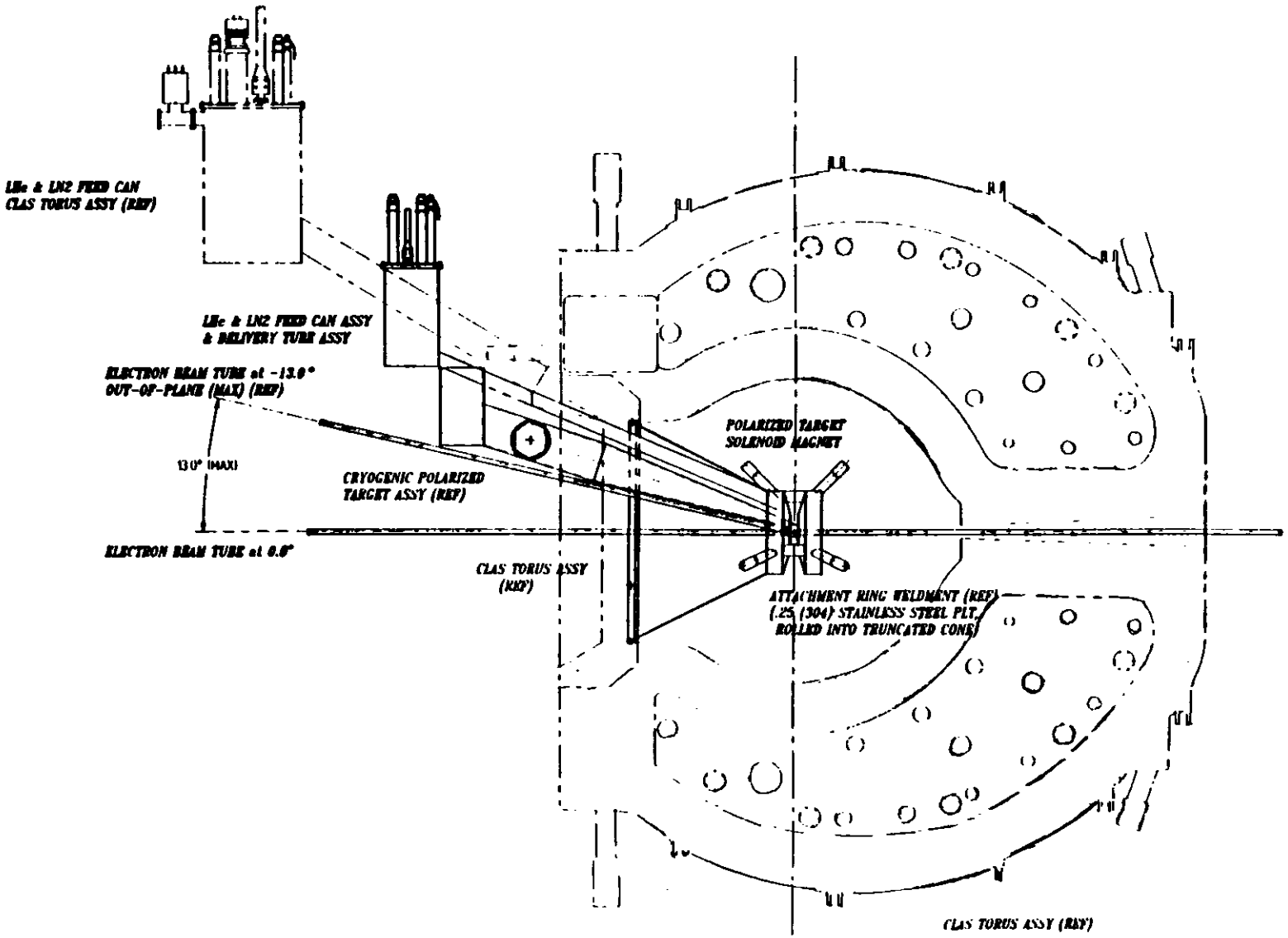
LHe & LN2 FEED CAN
CLAS TORUS ASSY (REF)
LHe & LN2 FEED CAN ASSY
& DELIVERY TUBE ASSY
ELECTRON BEAM TUBE at -13.0°
OUT-OF-PLANE (MAX) (REF)
13.0° (MAX)
CRYOGENIC POLARIZED
TARGET ASSY (REF)
ELECTRON BEAM TUBE at 0.0°
CLAS TORUS ASSY
(REF)
POLARIZED TARGET
SOLENOID MAGNET
ATTACHMENT RING WELDMENT (REF)
(.25 (304) STAINLESS STEEL PLT,
ROLLED INTO TRUNCATED CONE)
CLAS TORUS ASSY (REF)

Figure 13

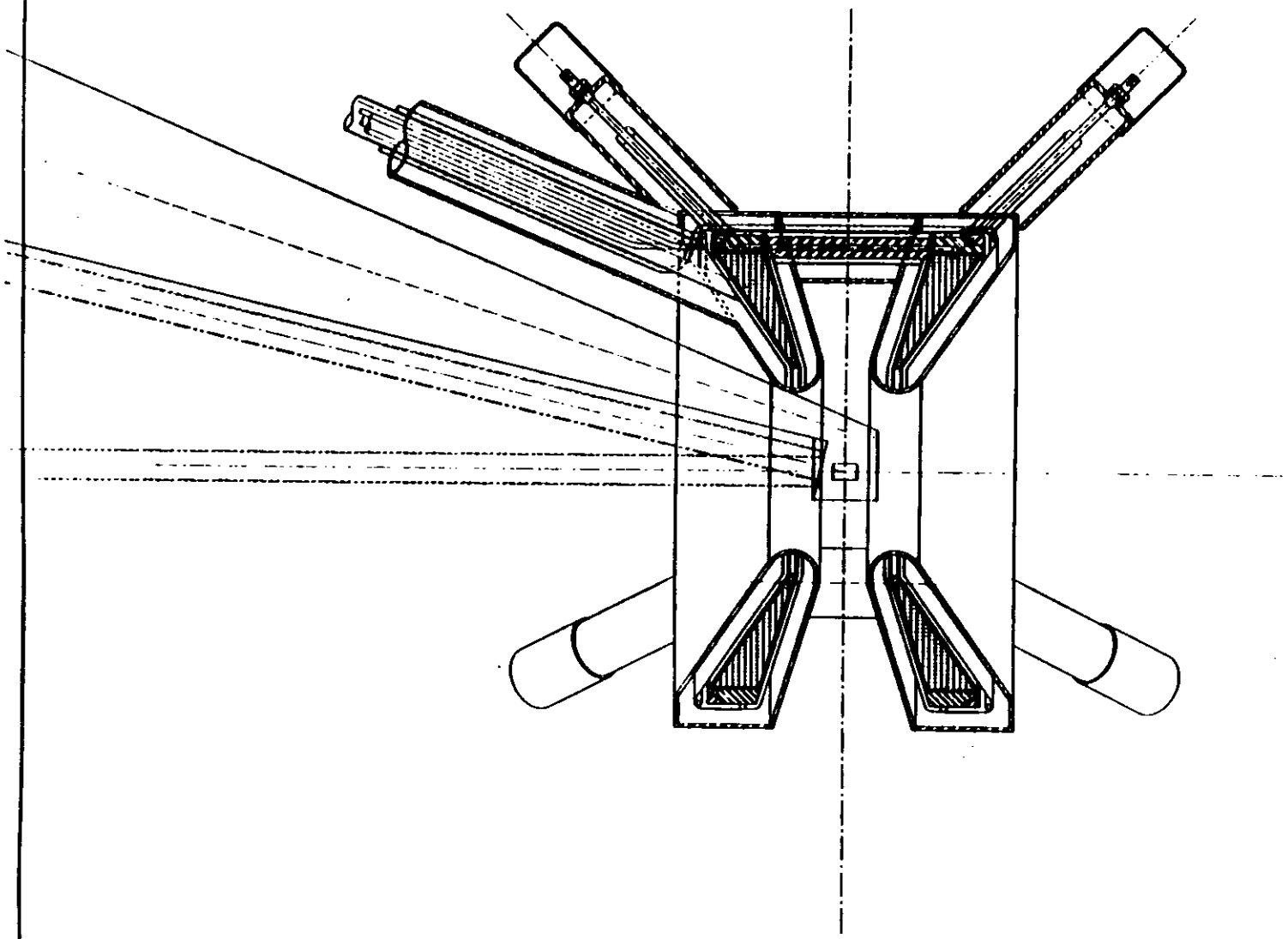

Figure 14